fMRI detects bilateral brain network activation following unilateral chemogenetic activation of direct striatal projection neurons

Yuki Nakamura, Yukari Nakamura, Assunta Pelosi, Boucif Djemai, Clément Debacker, Denis Hervé, Jean-antoine Girault, Tomokazu Tsurugizawa

NeuroImage 220 (2020) 117079

Contents lists available at ScienceDirect

NeuroImage

journal homepage: www.elsevier.com/locate/neuroimage

fMRI detects bilateral brain network activation following unilateral chemogenetic activation of direct striatal projection neurons

Yuki Nakamura [a,b,c], Yukari Nakamura [a,b,c,d], Assunta Pelosi [a,b,c], Boucif Djemai [e], Clément Debacker [e], Denis Hervé [a,b,c], Jean-Antoine Girault [a,b,c,**], Tomokazu Tsurugizawa [e,f,*]

[a] Inserm UMR-S 1270, 75005, Paris, France
[b] Sorbonne Université, Faculty of Sciences and Engineering, Paris, France
[c] Institut du Fer à Moulin, 75005, Paris, France
[d] Department of Pharmacology, Kurume University School of Medicine, 67 Asahi-machi, Kurume, Fukuoka, 830-0011, Japan
[e] NeuroSpin, Commissariat à l'énergie Atomique et Aux énergies Alternatives, 91191, Gif-sur-Yvette, France
[f] Human Informatics and Interaction Research Institute, National Institute of Advanced Industrial Science and Technology (AIST), Tsukuba, Ibaraki, 305-8568, Japan

ARTICLE INFO

Keywords:
Designer receptors exclusively activated by designer drugs
Magnetic resonance imaging
Clozapine
Clozapine-N-Oxide
Striatum
Drd1-receptor-expressing striatal projection neurons

ABSTRACT

Abnormal structural and functional connectivity in the striatum during neurological disorders has been reported using functional magnetic resonance imaging (fMRI), although the effects of cell-type specific neuronal stimulation on fMRI and related behavioral alterations are not well understood. In this study, we combined DREADD technology with fMRI ("chemo-fMRI") to investigate alterations of spontaneous neuronal activity. These were induced by the unilateral activation of dopamine D1 receptor-expressing neurons (D1-neurons) in the mouse dorsal striatum (DS). After clozapine (CLZ) stimulation of the excitatory DREADD expressed in D1-neurons, the fractional amplitude of low frequency fluctuations (fALFF) increased bilaterally in the medial thalamus, nucleus accumbens and cortex. In addition, we found that the gamma-band of local field potentials was increased in the stimulated DS and cortex bilaterally. These results provide insights for better interpretation of cell type-specific activity changes in fMRI.

1. Introduction

Pathological changes in the striatum contribute to a wide variety of neurological disorders including Parkinson's disease (PD) and L-DOPA-induced dyskinesia (LID), which are abnormal involuntary movements developed in PD patients after several years of treatment with L-3,4-dihydroxyphenylalanine (L-DOPA), the gold-standard treatment for this disease (Albin et al., 1989). The dorsal striatum (DS), the main input nucleus in basal ganglia circuits, receives afferents from the cerebral cortex and thalamic nuclei, and plays a central role in motor control (Tepper et al., 2007; Belin et al., 2009). The striatal projection neurons (SPNs, a.k.a. medium-size spiny neurons or MSNs) in the DS are inhibitory GABAergic neurons that account for ~95% of the striatal neurons in rodents and are the only striatal output. The DS SPNs are schematically categorized into two populations according to their projection sites and the genes they express: the dopamine D1 receptor-expressing SPNs (D1-SPNs) and the D2 receptor-expressing SPNs (D2-SPNs) (Gerfen et al., 2011; Valjent et al., 2009). D1-SPNs project directly to the substantia nigra (SN) and internal globus pallidus (GPi), forming the direct pathway. When they fire, they inhibit tonically active nigrothalamic and pallidothalamic GABA neurons, leading to the disinhibition of thalamus and other targets (Chevalier and Deniau, 1990). Conversely, D2-SPNs project to the external globus pallidus (GPe) which also regulates the SN and GPi, but indirectly via its projections to the subthalamic nucleus. This set of connected neurons forms the indirect pathway. Activation of the direct pathway promotes movement, while activation of the indirect pathway inhibits movement (Nelson and Kreitzer, 2014).

Motor deficits in PD are proposed to result from an overactive indirect pathway and underactive direct pathway (Mallet, 2006; Bergman, 1990; Kravitz, 2010). In contrast, LID is thought to result from hyperactivity of direct pathway (Cenci et al., 2007; Murer et al., 2011). Experimental approaches for manipulating specific neurons have been developed such as optogenetics with channelrhodopsins or chemogenetics with designer receptor exclusively activated by designer drugs (DREADDs, Roth et al., 2016). Using these techniques, specific manipulation of D1-or D2-SPNs

* Corresponding author. NeuroSpin, Commissariat à l'Energie Atomique-Saclay Center, 91191, Gif-sur-Yvette, France.
** Corresponding author. Institut du Fer à Moulin, Inserm UMR-S1270, 17, rue du Fer à Moulin, 75005, Paris, France.
E-mail addresses: jean-antoine.girault@inserm.fr (J.-A. Girault), tsurugizawa@gmail.com (T. Tsurugizawa).

https://doi.org/10.1016/j.neuroimage.2020.117079
Received 21 February 2020; Received in revised form 23 May 2020; Accepted 18 June 2020
Available online 23 June 2020

Abbreviations

AAV	adeno-associated virus
ANOVA	analysis of variance
BLP	band limited power
BOLD	blood-oxygen-level dependent
CLZ	clozapine
CM/Pf	center median/parafascicular
CNO	clozapine-N-oxide
D1	dopamine D1 receptor (Drd1)
D1-SPN	Drd1-expressing SPN
DREADD	designer receptor exclusively activated by designer drugs
Drd1::Cre	Cre under the control of *Drd1* promoter
D2	dopamine D2 receptor (Drd2)
D2-SPN	Drd2-expressing SPN
DS	dorsal striatum
fALFF	fractional amplitude of low frequency fluctuation
FC	functional connectivity
FD	frame-wise displacement
GPe	external globus pallidus
GPi	internal globus pallidus
Gq-DREADD	Gq-coupled DREADD
L-DOPA	L-3,4-dihydroxyphenylalanine
LFP	local field potential
LID	L-DOPA-induced dyskinesia
MC	motor cortex
MD	mediodorsal thalamic nucleus
MRI	magnetic resonance imaging
NAc	nucleus accumbens
PD	Parkinson's disease
pERK	phosphorylated ERK1/2
RARE	rapid acquisition with relaxation enhancement
ROI	region of interest
rsfMRI	resting state functional magnetic resonance imaging
SC	somatosensory cortex
SN	substantia nigra
SPN	striatal projection neuron
ThN	thalamic nuclei
VM	ventromedial nuclei

has been reported in rodent models of PD and LID. Bilateral optogenetic excitation of D2-SPNs elicits a parkinsonian-like state with increased freezing, bradykinesia and decreased movement initiation (Kravitz et al., 2010). In a mouse model of PD, optogenetic stimulation of D1-SPNs completely eliminates motor deficits (Kravitz et al., 2010). Similar results have also been reported using DREADDs. In a PD mouse model, D1-SPN stimulation via Gq-coupled DREADD (Gq-DREADD) has therapeutic-like effects, restoring a normal use of the parkinsonian limb in the cylinder test (Alcacer et al., 2017). In a LID mouse model, chemogenetic stimulation of D1-SPNs exacerbated dyskinetic responses to L-DOPA, while stimulation of D2-SPNs inhibits these responses (Alcacer et al., 2017). These results indicate that specific manipulation of D1-or D2- SPNs can induce or reduce PD or LID symptoms, attesting to their strong involvement in these motor disorders.

Resting-state fMRI (rsfMRI) in PD patients has provided evidence of decreased functional connectivity and network efficiency in the basal ganglia, thalamus and several cortical areas (Gottlich et al., 2013; Wei et al., 2014; Nagano-Saito et al., 2014; Luo et al., 2015 Rolinski et al., 2015). A pattern of fractional amplitude of low frequency fluctuations (fALFF) specific to PD patients has been identified with a 91% sensitivity and 89% specificity (Wu et al., 2015). However, despite evidence for the utility of neuroimaging in assessing parkinsonian patients, its routine use in clinical practice is still limited because of variations in age, treatment and disease severity and duration. Since a recent study reported similar resting-state networks in rodent and human brains (Sierakowiak et al., 2015), it appears that studying fMRI in rodents can be a valuable approach for translational research in brain disorders. Considering the prominent contribution of D1-SPNs to PD and LID symptoms, the study of effects of specific D1-SPN stimulation on rsfMRI signal and relevant behavior could provide new insight into the pathophysiology of these disorders, potentially leading to the development of better diagnosis and treatment for the human disorders.

Optogenetic or chemogenetic fMRI experiments have been performed in rodents to investigate the role of specific cell types in whole brain networks (Lee et al., 2016; Giorgi et al., 2017; Roelofs et al., 2017). fMRI changes have been previously investigated following optogenetic stimulation of D1-SPNs in the DS (Lee et al., 2016; Bernal-Casas et al., 2017), but not after chemogenetic stimulation. Optogenetic stimulation can impose spiking discharge patterns independently of neuron-afferent stimuli and manipulate cell activity in the millisecond-order (Boyden et al., 2005). However, this approach generates susceptibility artifacts in fMRI due to the presence of optical fibers, and light stimulation can induce heat and vascular responses (Rungta et al., 2017; Christie et al., 2013; Schmid et al., 2017). Furthermore, light delivery into the striatum activates by itself an inwardly rectifying potassium conductance and induces biased rotational behavior (Owen et al., 2019). In contrast, chemogenetic activation does not induce any spiking discharge *per se*, but increases the response of DREADD-expressing neurons to depolarizing stimuli (Alcacer et al., 2017). This approach is ideal for prolonged enhancement of neuronal activity in the range of minutes to hours in rsfMRI without issues of susceptibility artifacts or heating (Armbruster et al., 2007; Alexander et al., 2009). Recent work suggests that DREADD stimulation with low doses of clozapine (CLZ) is faster and at least as efficient as clozapine-N-oxide (CNO), a previously used ligand (Gomez et al., 2017).

In this study, we investigated the alterations in rsfMRI and behavioral changes induced by unilateral activation of D1-SPNs in the DS using the excitatory Gq-DREADD (also termed hM3D) activated by CLZ. We also present comparative results with CNO. We found that fALFF was increased bilaterally in the thalamus, nucleus accumbens (NAc) and cerebral cortex following unilateral activation of D1-SPNs. We confirmed using electrophysiology that these fALFF changes reflect effects on spontaneous neural activity (Zou et al., 2008), by showing alterations of the neuronal activity power in the regions where fALFF was changed.

2. Method

2.1. Experimental subjects and drugs

We used male and female heterozygous BAC *Drd1*::Cre transgenic mice, GENSAT project, EY262 line expressing Cre recombinase under the control of the dopamine D1 receptor gene (*Drd1*) promoter. Mice were on a C57BL/6J genetic background and approximately 12 weeks old at the beginning of the experiments. We also used 12-week-old C57BL/6JRj mice purchased from Janvier Laboratories (France). Mice were housed under a 12-h light/12-h dark cycle with free access to food and water. CLZ (Sigma-Aldrich) was dissolved in DMSO with a final concentration of 0.01% v/v in saline (0.9% NaCl solution). CNO (ENZO Life sciences) was dissolved in saline. CLZ (0.1 mg/kg, i.p.), CNO (2 mg/kg, i.p.) or saline (i.p.) were administered to mice at a volume of 10 ml/kg body weight. All animal procedures used in the present study were approved by the *Ethical committee for animal experiments* (*Comité d'Ethique en Expérimentation Animale, Commissariat à l'Energie Atomique et aux Énergies Alternatives, Direction des Sciences du Vivant*, Fontenay-aux-Roses, France) and by the

Ministère de l'Education Nationale de l'Enseignement Supérieur de la Recherche, France (project APAFIS#8196–201704201224850 v1). All methods in this study were performed in accordance with the relevant guidelines and regulations.

2.2. Viral vector injections

2.2.1. Stereotaxy and injection procedures

Drd1::Cre mice were stereotactically injected with adeno-associated virus (AAV) vectors in the left DS (Fig. 1A–C). Mice were anesthetized with a mix of ketamine (80 mg/kg) and xylazine (10 mg/kg) and mounted on a stereotaxic apparatus (Kopf, France). Cre-inducible AAV vectors coding for Gq-DREADD, pAAV8-hSyn-DIO-hM3D(Gq)-mCherry (Addgene, Cambridge, MA), or mCherry, pAAV8-hSyn-DIO-mCherry (Addgene, Cambridge, MA), were unilaterally injected into the left DS of *Drd1*::*Cre* mice. Two injections (0.5 µl each) in the left DS were performed at the following coordinates based on the Allen Brain Atlas: AP 1.0 mm, ML -1.5 mm, DV -3.3 mm and AP 0.3 mm, ML -2.0 mm, DV -3.5 mm from the bregma (Fig. 1C). All injections were performed using a 10 µl Hamilton Neuros 33G syringe at a flow rate of 0.2 µl/min. The needle was left in place for 2 min before and 5 min after the injection and then slowly retracted. Mice were placed in their home cage for more than 2 weeks for recovery.

2.2.2. Groups of AAV-microinjected mice

In the "Gq-DREADD" mouse group, we unilaterally injected Cre-dependent Gq-DREADD-AAV in the DS of *Drd1::Cre* mice. In a "mCherry" control group, Cre-dependent mCherry-AAV was injected in *Drd1::Cre* mice.

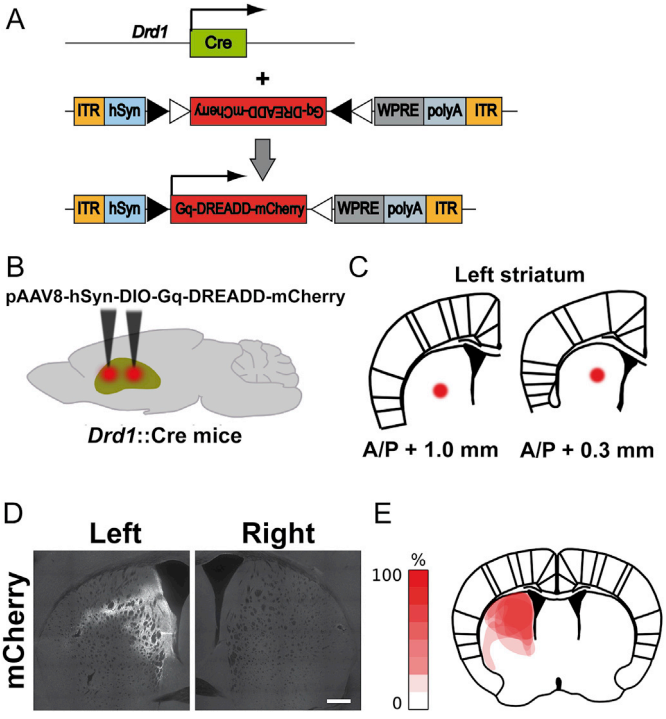

Fig. 1. Gq-DREADD expression.
A. Schematic representation of *Drd1*::Cre transgene and AAV expressing Gq-DREADD-mCherry based on the DiO (double floxed inverse orientation) system [pAAV8-hSyn-DIO-Gq-DREADD-mCherry]. **ITR**, inverted terminal repeats; **hSyn**, human synapsin promoter; **WPRE**, woodchuck post-transcriptional regulatory element. **B.** and **C.** Schema illustrating the two AAV injection sites in the striatum. Cre-inducible AAV vector coding for Gq-DREADD-mCherry (as indicated) or mCherry alone was unilaterally injected into the left DS of *Drd1::Cre* transgenic mice. **A/P**, anterior/posterior distance from bregma (mm). **D.** mCherry immunostaining in the striatum of a representative mouse. Scale bar, 500 µm. **E.** Map of overlap percentage of Gq-DREADD-mCherry expression areas across mice used for fMRI study (n = 8).

2.3. Rotation test

2.3.1. Groups and treatments for behavioral studies

For behavioral studies, we investigated the Gq-DREADD and mCherry groups and compared them with two additional control mouse groups: the "D1-Cre" group, comprised of *Drd1::Cre* mice without AAV injection and the "C57BL/6J" group, comprised of C57BL/6JRj mice which did not receive any transgene or AAV injection. Seven Gq-DREADD, 5 D1-Cre, 7 mCherry, and 8 C57BL/6J mice were administered with saline, CLZ or CNO to evaluate the DREADD-dependent and independent effects of these treatments as well as the non-specific effects of virus injection.

2.3.2. Test procedure

The number of 360° rotations and the horizontal locomotion were measured three weeks after surgery. To assess turning movements and locomotion, mice were placed individually inside a transparent plastic cylinder (20 cm diameter, 15 cm height) 60 min before drug or saline administration and video-recorded. They were then injected with CLZ (0.1 mg/kg, i.p.), CNO (2 mg/kg, i.p.) or saline (i.p.) and video-recorded for 60 additional minutes. The dose of CLZ and CNO was determined from previous reports (Gomez et al., 2017; Alexander et al., 2009). Mice were returned to their home cages for 60 min and then (i.e. 120 min after injection) they were placed back in their respective cylinders, where they were video-recorded for another 60 min. Video recordings were used to visually count the number of clockwise (right, contralateral rotations to the virus-injected side) and anticlockwise (left, ipsilateral rotation to the virus-injected side) full turns. Analysis of rotation was performed manually by an observer blind to the treatment and mouse group. The mice were tested for 4 consecutive days: the first 2 days, saline or CLZ were injected, 24 h apart and the next 2 days, saline or CNO were injected 24 h apart. On the first day of each session, half of the mice received CLZ or CNO and the other half received saline. Data were collected in 10-min bins.

2.4. fMRI

2.4.1. Mouse groups and drug treatments for fMRI

For fMRI study, 8 Gq-DREADD and 8 C57BL/6J mice were used following the behavioral assessments. Each group of mice was treated with CLZ (Gq-DREADD-CLZ, C57BL/6J-CLZ), CNO (Gq-DREADD-CNO, C57BL/6J-CNO) or saline (Gq-DREADD-saline, C57BL/6J -saline), and termed accordingly.

2.4.2. fMRI procedure

fMRI acquisition was conducted in a Bruker 7T system with a 4-channel mouse brain array coil (Bruker BioSpin, Ettlingen, Germany). Each mouse was lightly anesthetized with isoflurane (1.5% for induction and 0.8–1.0% for maintenance) in air containing 30% O_2. The head was fixed with ear-bars and a tooth-bar. The fMRI acquisition started about 10 min after switching to 0.8–1.0% isoflurane. The respiratory rate was between 80 and 120/min as measured with a small pneumatic pillow placed under the animal's abdomen (model 1025; SA Instruments, NY, USA) and rectal temperature was maintained at 37 °C during the measurement by circulating hot water. Scanning was started 25 min following CLZ (0.1 mg/kg, i.p.) or saline (i.p.) injection, and 95 min following CNO injection (2 mg/kg, i.p.). Each mouse received CLZ, CNO or saline on different days and the injection sequence was randomized. The dose of CLZ and CNO was the same as for behavioral tests. The scanning time was determined from the results of rotation behavior in the cylinder test, electrophysiology and a published report (Gomez et al., 2017). After correction of the field homogeneity, structural T2-weighted images were acquired for 4 min. Then the rsfMRI acquisition was launched. The rsfMRI images were acquired using a T2*-weighted multi-slice gradient-echo EPI sequence with the following parameters: TR/TE = 2000/15 ms, spatial resolution = 150 ×

150 × 700 μm^3, 180 vol (total 6 min). rsfMRI acquisition was started at 45 min and 115 min following CLZ and CNO injection, respectively. T2* at 7T was around 25 ms but we used TE = 15 ms (DiFrancesco et al., 2008; Seehafer et al., 2010). Since the 4-channel mouse brain array coil showed a lower signal-to-noise ratio in the lower part of the brain with long TE, we used TE = 15 ms to get a good signal-to-noise ratio in these brain structures. We chose a scanning time of 6 min based on previous studies (Turner et al., 2013; Xue et al., 2017; Huang et al., 2017). For normalization in image processing, the structural image with the same field of view as the fMRI was acquired using T2-weighted multi-slice rapid acquisition with relaxation enhancement (RARE) with the following parameters: TR = 2500 ms, effective TE = 13 ms, spatial resolution = 100 × 100 × 500 μm^3, RARE factor = 4, and 4 averages. After fMRI study, mice were sacrificed and processed for immunohistofluorescence to check the location of viral infection within the striatum.

2.5. Image processing

The rsfMRI data analysis toolkit (REST1.8, Lab of Cognitive Neuroscience and Learning, Beijing Normal University, China) and statistical parametric mapping (SPM)8 software (Wellcome Trust Center for Neuroimaging, UK) were used to analyze the fMRI data and to perform the preprocessing, including the slice timing correction, motion correction by realignment, co-registration and normalization. Before preprocessing, a template image co-registered with Allen mouse brain atlas was obtained (http://atlas.brain-map.org/). The functional and structural images were normalized to these template images. Framewise displacement (FD) was used to check head motion (Power et al., 2013). FD was calculated for 6 motion parameters (3 for translation and 3 for rotation) from realignment in SPM. For all subjects, we checked that the head motion was less than the criteria: (1) mean FD averaged for all time-points during the scanning was less than 0.02 mm and (2) FDs at all time-points were less than 0.05 mm. Mean FD was not significantly different between groups. The linear trend in the time course of the fMRI dataset was removed voxel-by-voxel using the REST toolbox (Song et al., 2011). Mean signals in the ventricles and white matter, and six motion parameters of an object (the translational and rotational motions) were regressed-out from the time-series of each voxel to reduce the contribution of physiological noise, like respiration and head movement.

2.6. fALFF

The preprocessed data were then smoothed with a Gaussian filter (0.3 × 0.3 mm^2 in each slice). The smoothed images were used for all subsequent analyses in fALFF. The fALFF was defined as the ratio of power within the frequency range between 0.01 and 0.1 Hz and power over the total frequency range in each voxel and used to generate a fALFF map for each mouse. The fALFF maps were then compared and significant differences between groups were tested voxel-by-voxel using a one-way analysis of variance (ANOVA) test with standard progressive matrices with a threshold of $p < 0.05$ (FDR at cluster level). Since there were no significant differences in fALFF between the 4 control groups (Gq-DREADD-saline, C57BL/6-CLZ, C57BL/6-CNO, and C57BL/6-saline groups), we used these 4 groups as a pooled control group for comparison to the Gq-DREADD-CLZ or Gq-DREADD-CNO group. The sum of weights of the contrast was zero, reflecting the null hypothesis that the experimental manipulation had no effect. For example, the weight of contrast for Gq-DREADD-CLZ > Gq-DREADD-saline group was [Gq-DREADD-CLZ, Gq-DREADD-saline] = [1, −1] and the weight of contrast for Gq-DREADD-CLZ > control group was [Gq-DREADD-CLZ, Gq-DREADD-saline, C5BL6J-CLZ, C5BL6J-saline] = [1, −1, −1, 1].

2.7. Functional connectivity (FC)

FC was calculated using the same dataset as for fALFF. The preprocessed fMRI data were then de-trended and slow periodic fluctuations were extracted using a bandpass filter (0.01–0.1 Hz). The residuals resulting from this regression were then smoothed with a Gaussian filter (0.3 × 0.3 mm^2 in each slice). A total of 92 regions-of-interest (ROIs, 46 per hemisphere) were delineated based on the template images, with reference to the Allen mouse brain atlas (https://scalablebrainatlas.incf.org/mouse/ABA12). The correlation coefficients between two ROIs were calculated using the REST toolbox (Song et al., 2011). Statistical significance of ROI-ROI connectivity was assessed by one-way ANOVA test with a threshold of $p < 0.05$ (FDR-corrected), using a Network-Based Statistic toolbox (https://www.nitrc.org/projects/nbs/). The weights of contrast were used as for fALFF: for example, the weight of contrast for Gq-DREADD-CLZ > Gq-DREADD-saline group was [Gq-DREADD-CLZ, Gq-DREADD-saline] = [1, −1] and the weight of contrast for Gq-DREADD-CLZ > control group was [Gq-DREADD-CLZ, Gq-DREADD--saline, C5BL6J-CLZ, C5BL6J-saline] = [1, −1, −1, 1].

2.8. Electrophysiology

2.8.1. Mouse groups and treatments for electrophysiology

For electrophysiology, 5 or 7 Gq-DREADD and 5 mCherry mice were used. Each group of mice was treated with CLZ (Gq-DREADD-CLZ, mCherry-CLZ) or saline (Gq-DREADD-saline, mCherry-saline).

2.8.2. Electrophysiological recordings

Electrophysiological recordings were performed outside of the MRI bore (Tsurugizawa et al., 2019). The animals were first anesthetized with 1.5% isoflurane and then placed in a stereotaxic frame (David Kopf instrument, CA). Body temperature was maintained at 37 °C using a heating pad (DC temperature controller; FHC Inc., Bowdoin, ME, USA). The skull was exposed and a hole (1 mm diameter) was drilled to insert the micro-electrode. Tungsten microelectrodes (<1.0 MΩ, with 1-μm tip and 0.127-mm shaft diameter, Alpha Omega Engineering, Nazareth, Israel) were positioned in the left DS (AP 0 mm, ML -1.8 mm, DV -3.5 mm from the bregma) or in the left and right motor cortices (AP 0 mm, ML ±1.5 mm, DV -1.5 mm from the bregma). The electrode was inserted in the left DS at a position between the two sites of AAV injection, corresponding to the area in which fALFF was significantly increased by CLZ administration compared to saline injection in Gq-DREADD mice. After surgery, isoflurane concentration was lowered to 0.8–1.0%, which was the same concentration as for the fMRI experiments. The electrode was connected to a differential AC amplifier Model 1700 (AM systems, Sequim, WA, USA), via a Model 1700 head stage (AM systems, Sequim, WA, USA). Local field potentials (LFPs) were continuously recorded at a 10-kHz sampling rate using dedicated data acquisition software (Power Lab, AD Instruments, Dunedin, New Zealand). CLZ or saline was injected 5 min after the start of the recording. Recording was then continued for 51 min (total recording time, 56 min). Total LFP recording included two sessions with saline injected during the first session and CLZ during the second session. The reference electrode was positioned on the scalp.

2.8.3. Band limited power (BLP) analysis

From LFP signal, five BLP time series were calculated: delta (1–4 Hz), theta (4–8 Hz), alpha (8–12 Hz), beta (18–30 Hz) and gamma (60–100 Hz) using PowerLab (AD Instruments, Dunedin, New Zealand) (Hacker et al., 2017; Thompson et al., 2013; Tsurugizawa et al., 2019). Although gamma BLP is generally defined as 30–100 Hz, we calculated gamma frequency between 60 and 100 Hz to remove the contamination of the humbug noise around 50 Hz. The mean power of each frequency band in the left (ipsilateral to the Gq-DREADD-expressing side) DS and in the left and right motor cortices was calculated during 45–51 min after the injection of saline or CLZ.

2.9. Immunofluorescence

Mice were rapidly and deeply anesthetized with pentobarbital (500 mg/kg, i.p., Dolethal, Vetoquinol, France) and perfused transcardially

with 4% (weight/vol) paraformaldehyde in 0.1 M sodium phosphate buffer for 15 or 120 min following CLZ or CNO administration. Brains were post-fixed overnight at 4 °C and cut into free-floating sections (30 μm) with a vibrating microtome (Leica) and kept at −20 °C in a solution containing 30% ethylene glycol (vol/vol), 30% glycerol (vol/vol) and 0.1 M phosphate buffer. Immunolabeling procedures were as previously described (Valjent et al., 2000). After three 10-min washes in Tris-buffered saline (TBS, 0.10 M Tris and 0.14 M NaCl, pH 7.4), free-floating brain sections were incubated for 5 min in TBS containing 3% H_2O_2 and 10% methanol, and rinsed again in TBS 3 times for 10 min. Brain sections were then incubated for 15 min in 0.2% (vol/vol) Triton X-100 in TBS, rinsed 3 times in TBS and were blocked in 3% (weight/vol) bovine serum albumin in TBS, and then incubated overnight at 4 °C with primary antibody diluted in the same blocking solution. Sections were then washed three times in TBS for 15 min and incubated 1 h with secondary antibodies. After washing again, sections were mounted in Vectashield (Vector laboratories). For detection of phosphorylated proteins, 0.1 mM NaF was included in all buffers and incubation solutions. Primary antibodies were rabbit antibodies against phospho-Thr202/Tyr204-ERK1/2 (1:400; Cell Signaling Technology, #9109S), chicken antibodies against mCherry (1:1500; Abcam, #ab205402). Secondary antibodies were anti-rabbit A488 antibody (1:400, Invitrogen, #A-21206) and anti-chicken Cy3 antibody (1:800; Jackson Immuno Research, #703-165-155). Images were acquired using a confocal microscope (Leica SP5) with a 63X objective.

3. Results

3.1. Validation of Gq-DREADD expression and functionality in the striatum

We confirmed the successful AAV-transduction and Gq-DREADD-mCherry fusion protein expression in the left DS using mCherry immunostaining (Fig. 1D). No immunostaining was detected in the right DS. In all mice used for the fMRI study (n = 8), Gq-DREADD-mCherry was expressed in the medial part of the DS (Fig. 1E). The functionality of the receptor was assessed by immunostaining for phosphorylated ERK1/2 (pERK), a downstream target of Gq-DREADD, 15 min after saline or CLZ administration. A pronounced pERK immunoreactivity was observed in the left DS following CLZ, but not saline administration (Fig. 2). Numerous pERK-positive neurons were seen following CLZ in the striatal area with intense mCherry immunoreactivity, an indication of the infection by the Gq-DREADD-expressing AAV. In contrast, no pERK-positive cell bodies could be detected in the contralateral striatum or in both the infected and non-infected striatum of saline-treated mice. A thorough examination of pERK-positive cell bodies after CLZ treatment showed that they systematically expressed mCherry, at least at the plasma membrane (Supplementary Fig. 1A and B). Depending on the AAV infection, the localization of mCherry varied. In neurons expressing mCherry at high levels, it was present in both cytoplasm and at the plasma membrane. In this case, the co-localization of pERK and mCherry was obvious because pERK-immunoreactivity was also high in the cytoplasm. In some pERK-positive neurons, mCherry expression was lower, but mCherry immunoreactivity was systematically detected at the plasma membrane. Virtually no pERK-positive neurons were devoid of mCherry expression. Immunofluorescence for pERK in the Gq-DREADD-expressing area diminished at 120 min after CLZ administration. In contrast, strong immunostaining was observed 120 min after CNO administration (Supplementary Fig. 1C). Only a background level of pERK immunostaining was detected in the right DS following CLZ or CNO injection.

3.2. Behavioral effects of unilateral stimulation of D1-SPNs with Gq-DREADD

We examined the effects of chemogenetic D1-SPN activation on whole-body movements by counting the number of left and right

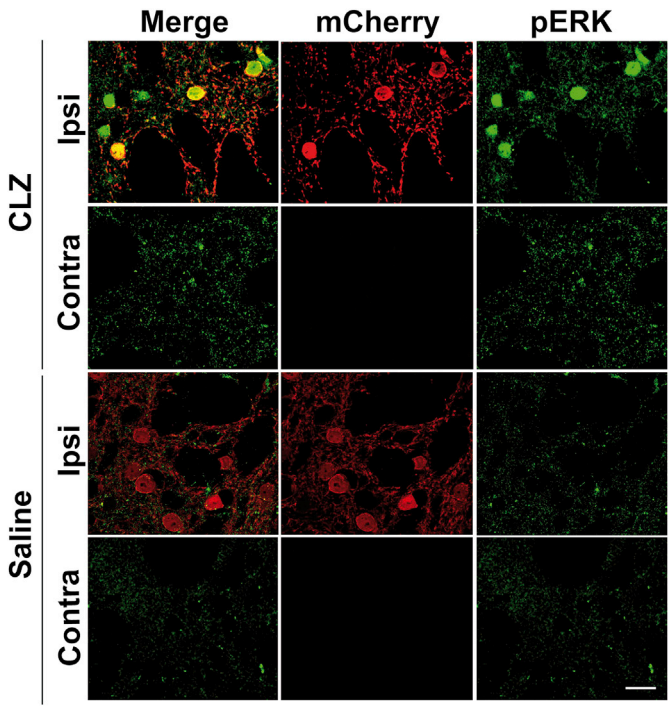

Fig. 2. CLZ-induced ERK activation in Gq-DREADD expressing SPNs. Double immunolabeling of mCherry (red) and phosphorylated ERK1/2 (pERK, green) in the left (**Ipsi**, ipsilateral to the virus injection) or right (**Contra**, contralateral) DS 15 min after **CLZ** (0.1 mg/kg) or **saline** vehicle i.p. injection. Merged confocal images demonstrate co-localization of Gq-DREADD-mCherry and pERK in the left DS of CLZ-treated mice but not in saline-treated mice. Images were acquired from *Drd1::Cre* transgenic mice injected in the DS with Cre-inducible AAV vectors coding for the Gq-DREADD-mCherry [pAAV8-hSyn-DIO-Gq-DREADD-mCherry]. Scale bar, 20 μm.

rotations before the fMRI study (Fig. 3A and B). Unilateral D1-SPN activation increased the number of contralateral rotations as Alcacer et al. (2017) previously reported. The time course study of CLZ effects showed that the increase in rotations was maximal 20–30 min following CLZ (0.1 mg/kg) injection (Fig. 3C). No further differences were observed after 120 min. We also tested the effects of CNO (2 mg/kg) and found it produced less rotations and at a later time, with the maximum effects occurring 130–140 min after CNO injection (Supplementary Fig 2A).

We then tested whether these effects were actually caused by the stimulation of Gq-DREADD in the D1-SPN, and not by non-specific effects of AAV injection or treatment with CLZ or CNO. We compared rotations and locomotion in four different groups of mice (C57BL6J, D1-Cre, mCherry, and Gq-DREADD mice) following CLZ, CNO, and saline injection. We did not detect any significant bias in rotational behavior in the various control groups (C57BL6J, D1-Cre, and mCherry mice) after CLZ, CNO or saline treatment (Supplementary Fig. 2B). Importantly, we did not observe any preferential direction of rotation after saline injection in Gq-DREADD mice, showing that the expression of Gq-DREADD in D1-SPNs had no significant effect in the absence of stimulation by CLZ or CNO. Additionally, there was a slight increase in locomotion over the 120–180 min period after the injection of CNO in Gq-DREADD mice but no significant difference among the control groups (C57BL6J, D1-Cre and mCherry mice) following CLZ or CNO treatment (Supplementary Fig. 3). These results show that neither CLZ injection nor mCherry expression using an AAV by themselves affect rotational behavior or more generally locomotor activity. We conclude that DREADD-mediated unilateral activation of D1-SPNs triggers contralateral rotations.

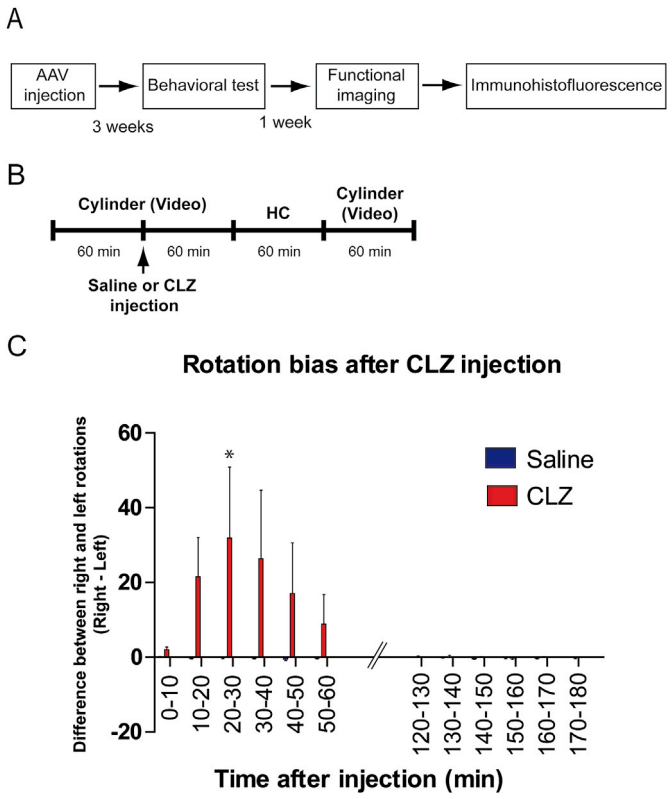

Fig. 3. Unilateral Gq-DREADD activation of D1-SPNs induces contralateral rotations.

A. Schematic outline of the experimental design. **B.** Schedule of behavioral testing. *Drd1::Cre* mice expressing Gq-DREADD in D1-SPNs of left DS were administered with saline or CLZ (0.1 mg/kg) 60 min after introduction in the test chamber (cylinder). Mice were returned to their home cage 60 min after injection and were placed back in their respective cylinder 120 min after injection. Mice were video-recorded in the cylinder. The distance traveled and number of right and left rotations were evaluated. **HC**, home cage. **C.** CLZ (0.1 mg/kg) induced contralateral rotation asymmetry (number of full turns per 10 min contralateral [right] to the AAV injection side minus ipsilateral [left] turns). Saline administration did not trigger rotational bias, hence the corresponding saline blue bars are not visible (see Supplementary Fig. 2). Maximum behavioral changes were observed between 10 and 50 min after CLZ injection. Saline or CLZ was injected in a counter-balanced design, 24 h apart. Data (mean + S.E.M, n = 8) were analyzed using repeated-measures two-way ANOVA: effect of time, $F_{(11,154)} = 2.34$, $p = 0.01$; effect of treatment, $F_{(1,154)} = 2.59$, NS; interaction, $F_{(11,154)} = 2.38$, $p = 0.0095$. *Post hoc* comparison, drug vs. saline, Bonferroni's test, $^{*}p \leq 0.05$.

3.3. Unilateral Gq-DREADD stimulation of D1-SPNs alters fALFF bilaterally in multiple forebrain regions

Following behavioral assessment, we studied fMRI in the same Gq-DREADD mice (Fig. 3A). Since the increase in contralateral rotations was observed in the 10–60 min period after CLZ injection (Fig. 3C), we acquired rsfMRI images at 45 min following saline or CLZ injection (Fig. 4A). The rotation bias was confirmed visually following CLZ injection before anesthetizing the animals. The raw fMRI images showed that there was no susceptibility artifact on the AAV-injected site (Fig. 4B). In CLZ-injected mice a significant increase in fALFF was observed in a small area of the left DS (Gq-DREADD-expressing area) as compared to saline-injected mice (Fig. 4C). Moreover, fALFF was bilaterally increased in cortical areas including the somatosensory cortex (SC) and motor cortex (MC) (Fig. 4C). fALFF was also increased in the medial thalamic nuclei (ThN) and both left and right NAc.

We also investigated fALFF changes following CNO compared to saline administration. Since CNO increased rotation bias 50–140 min after its administration, rsfMRI images were acquired at 115 min following CNO injection (Supplementary Fig. 4A). fALFF was increased by CNO injection compared to the saline group (measured at 45 min) in the same regions as after CLZ injection, with the exception of NAc, including left and right SC and MC, medial ThN and DS (Supplementary Fig. 4B). The averaged fALFFs in the four control groups (Gq-DREADD-saline, C57BL/6J-saline, C57BL/6J-CLZ and C57BL/6J-CNO groups) did not show any significant change (Supplementary Fig. 5A). We compared the Gq-DREADD-CLZ and Gq-DREADD-CNO groups with the control groups using ANOVA. Gq-DREADD-CLZ and Gq-DREADD-CNO groups showed significant fALFF increases in the same regions as those identified by the comparison of these groups with the Gq-DREADD-saline group (Supplementary Fig. 5B and 5C).

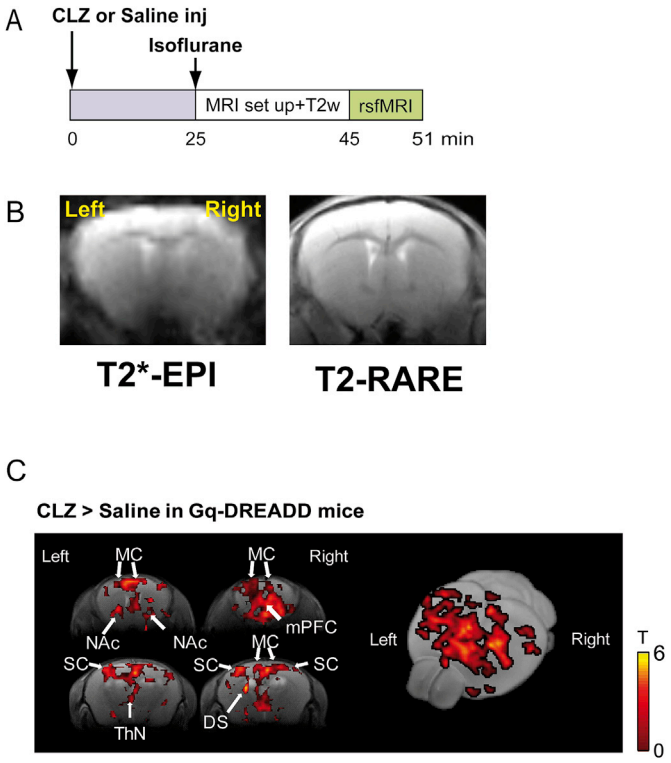

Fig. 4. Gq-DREADD-induced stimulation of D1-SPNs in the left DS increases fALFF bilaterally in forebrain.

A. fMRI experimental design. Saline or CLZ (0.1 mg/kg) was administered to the mice in their home cage. Mice were then lightly anesthetized with isoflurane before MRI scanning. Four-min T2 weighted image (T2w) followed by 6-min resting state fMRI (rs-fMRI) were scanned 41 min after saline or CLZ injection. **B.** Raw images of T2*-EPI and T2-RARE in the same mouse (+0.3 mm from bregma). **C.** Significant increase in fALFF following CLZ injection compared to the saline group ($p < 0.05$, FDR at cluster level). Four coronal sections (+1.0, upper right; +0.5, upper left; −1.0, lower right; −2.0, lower left; coordinates are in mm from bregma) are shown in left panels. In the right panel, 3-D reconstruction. Hue bar, t values (T). mPFC, medial prefrontal cortex; SC, somatosensory cortex; MC, motor cortex; DS, dorsal striatum; NAc, nucleus accumbens; ThN, thalamic nuclei.

In addition to fALFF, we investigated ROI-based functional connectivity after CLZ, CNO or saline injection (Supplementary Fig. 6). No significant difference was detected ($p > 0.05$, FDR-corrected in CLZ vs Saline or CNO vs Saline groups).

3.4. Alteration of band limited power (BLP) in the ipsilateral-DS and bilateral motor cortex after unilateral Gq-DREADD stimulation of D1-SPNs

To better characterize the fALFF results, we investigated the BLP changes following saline or CLZ injection in mice expressing Gq-DREADD in the left DS. The total LFP in Gq-DREADD-expressing DS started to

increase 10 min following CLZ injection, the increase becoming significant at 30 min and lasting until the end of LFP recording (51 min) (Fig. 5A). The delta and gamma BLP significantly increased in the left DS 45–51 min following the CLZ injection as compared to saline injection (Fig. 5B). In both left and right motor cortices, only the gamma BLP significantly increased 45–51 min following CLZ injection as compared to saline injection (Fig. 5C and D). Time course analysis indicated that the saline injection did not alter BLP in motor cortex or DS in any of the frequency bands, as compared with BLP before injection. We also assessed the effects of CLZ injection on neuronal activity in control mice injected with mCherry-AAV (Supplementary Fig. 7). In these mice, there was no significant change in ipsilateral DS or motor cortices following CLZ injection. These results strongly suggested that fALFF alterations were due to the increased activity in Gq-DREADD-expressing neurons stimulated by CLZ. All of the averaged BLPs in pre and post injection periods are shown in Supplementary Tables 1 and 2 These data corroborate our results comparing CLZ treatment with saline.

4. Discussion

In this study, we used "chemo-fMRI" to demonstrate that the prolonged unilateral activation of D1-SPNs in DS alters fALFF, presumably a reflection of neuronal activity, bilaterally in the cortex at the time of behavioral effects. Since chemo-fMRI does not use optical fibers and light stimulation to activate specific cells, there were no susceptibility artifacts in the T2*-weighted images, which is a significant advantage for fMRI studies. Behavioral and electrophysiological investigations allowed us to determine the time window of the maximum chemogenetic effects. We also demonstrate that the DREADD ligand, CLZ, at the doses we used, had negligible DREADD-independent pharmacological effects.

4.1. Different time course of CLZ and CNO-induced behavioral changes

Synthetic pharmacologically inert CNO has long been the ligand of choice for selectively activating DREADDs. (Roth et al., 2016). However, previous reports revealed different time courses of CNO-induced cellular activation in the brain and peripheral organs. The time course of CNO-evoked physiological effects in transgenic mice expressing Gq-DREADD (hM3D) in pancreatic β cells correlates with the plasma CNO concentration, with effects diminishing within 2 h (Guettier et al., 2009). In contrast, the behavioral and neuronal activity changes occur 30–40 min after CNO injection (0.3 mg/kg, i.p.) and these effects persist for 9 h (Alexander et al., 2009). This difference in time course of CNO-induced effects between brain and peripheral organs makes it difficult to use CNO to study behavioral changes induced by DREADD activation. It was recently proposed that the activation of DREADD-expressing neurons induced by systemic CNO administration was mainly due to CLZ, which is produced by the metabolic degradation of CNO, binds to DREADDs with higher affinity than CNO, and shows a higher ability to cross the blood brain barrier (Gomez et al., 2017). In the present study, we found that

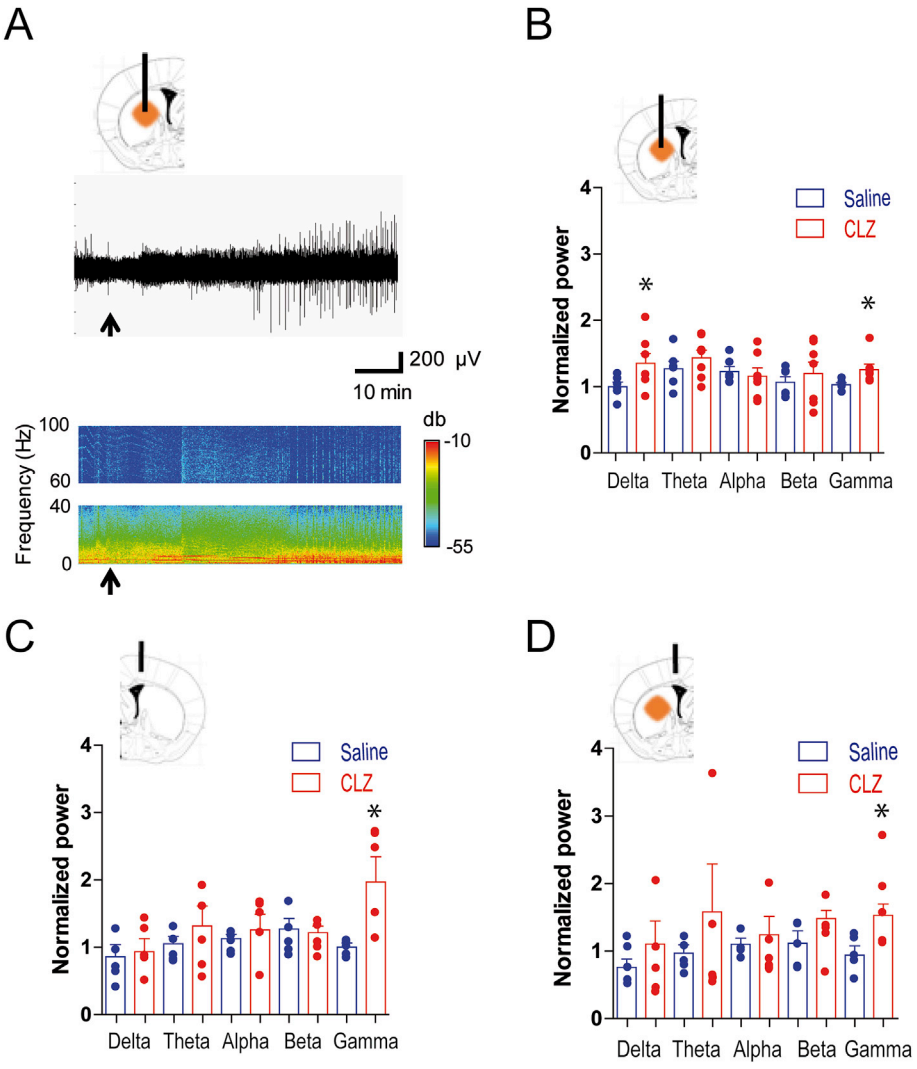

Fig. 5. Effects of Gq-DREADD-induced stimulation of D1-SPNs in the left DS on local field potential (LFP) band limited power (BLP).
A. LFP (middle panel) and power spectrum (lower panel) recorded in the left DS (ipsilateral to Gq-DREADD-expressing AAV injection, top scheme) following CLZ injection (0.1 mg/kg, black arrows) in a representative animal. Horizontal bar, time; vertical bar, LFP voltage; Hue bar, power (db). **B.** Normalized BLP (delta, theta, alpha, beta and gamma frequency bands) in the left DS after CLZ or saline injection as in A. Each normalized power was averaged between 45 and 51 min. Data points (n = 6–7) and means + SEM are shown. **C, D.** Normalized power in each BLP (delta, theta, alpha, beta and gamma frequency bands) in the right (C) and left (D) motor cortex. Each normalized power was averaged between 45 and 51 min. Data points (n = 5) and means + SEM are shown. Statistical analysis with repeated-measures two-way ANOVA: **B.** effect of frequency, $F_{(4,\ 40)} = 1.22$, NS, effect of treatment, $F_{(1,\ 55)} = 5.00$, $p = 0.029$, interaction, $F_{(4,55)} = 0.90$, NS. **C.** effect of frequency, $F_{(4,\ 40)} = 0.81$, NS, effect of treatment, $F_{(1,\ 40)} = 4.73$, $p = 0.036$, interaction, $F_{(4,40)} = 0.73$, NS. **D.** effect of frequency, $F_{(4,\ 40)} = 3.46$, $p = 0.016$, effect of treatment, $F_{(1,\ 40)} = 11.47$, $p = 0.0016$, interaction, $F_{(4,40)} = 1.11$, NS, respectively. *Post hoc* comparison, drug vs. saline, Bonferroni's test, $^*p \leq 0.05$.

CNO started to induce a rotation behavior 30–40 min after its administration (2 mg/kg, i.p.) in the Gq-DREADD-expressing mice and this alteration remained visible more than 2 h after injection. In addition, pERK immunostaining was observed in many Gq-DREADD-expressing cell bodies 120 min after CNO administration, indicating that these neurons were still activated. In contrast, CLZ (0.1 mg/kg) induced a clear rotation bias starting only 10 min after the injection. This behavioral effect peaked 20–30 min after injection and was no longer detectable at 2 h. In contrast to the late effects of CNO, pERK immunolabeling of Gq-DREADD-expressing D1-SPN cell bodies was observed 15 min after CLZ injection but not detected at 120 min. CNO (1 mg/kg, i.p.) is known to be continuously metabolized to CLZ during 6 h (MacLaren et al., 2016), consistent with our results which show that behavioral changes and increased pERK last at least 120 min after CNO injection.

In addition, CLZ and N-desmethylclozapine, which is another pharmacologically active metabolite of CNO, generated by relatively high doses, have the potential to influence behavior (Schaber et al., 1998; MacLaren et al., 2016). Thus, CNO effects can be variable depending on its metabolism, the injection dose, and the sedative effects of accumulated metabolized CLZ. In the present study, we selected a low dose of CLZ (0.1 mg/kg, i.p.), instead of high doses of CNO (2 mg/kg, i.p.), as a DREADD ligand for fMRI and LFP recordings because of its early and short effective time window that enabled us to take fMRI and LFP recordings at the time of behavioral change and to avoid long-time exposure to anesthesia. Importantly, we excluded DREADD-independent effects of CLZ (0.1 mg/kg, i.p.) by showing that this dose did not affect rotation bias or locomotion activity in control mice (Supplementary Fig. 2B and 3).

4.2. fALFF increase and neuronal activity

fALFF is related to the power of low-frequency electrical current oscillations caused by excitatory neuronal activity (Ma et al., 2016; Zou et al., 2008). We observed increased fALFF after CLZ administration in the basal ganglia-thalamo-cortical network including the medial part of thalamus and several cortical areas including the motor and somatosensory cortices, in accordance with the anatomical connectivity. Medial parts of the thalamus, including the ventromedial nucleus (VM), mediodorsal nucleus (MD), and center median/parafascicular (CM/Pf) complex, have direct and indirect anatomical connections to the striatum and cortex (Groenewegen et al., 1994). The VM receives afferents from the output structures of the basal ganglia (Herkenham, 1979; Kuramoto et al., 2011) and relays basal ganglia information to the cortex including motor areas (Kuramoto et al., 2015). The MD also receives projections from the basal ganglia, especially the internal segment of the globus pallidus and ventral pallidum, to which striatal neurons project (Mitchell et al., 2013). The CM/Pf complex is connected to the entire striatal complex and the CM/Pf-striatal system is a functionally organized network that may broadly affect motor basal ganglia functions. The CM/Pf complex seems to play a pivotal role in PD because this area is markedly degenerated in PD patients while deep brain stimulation of this nuclear group alleviates PD symptoms (Smith et al., 2014).

Remarkably, the unilateral stimulation of D1-SPNs in the DS increased fALFF bilaterally in the cortex and NAc. Results demonstrating bilateral consequences of unilateral manipulations of the basal ganglia circuit have been reported in previous studies. The unilateral lesion of the thalamic VM nucleus induced a decrease in glucose metabolism in several structures of both cerebral hemispheres in basal conditions (Girault et al., 1985). In addition, bilateral effects depending on VM integrity were also observed following stimulation of the nigrothalamic pathway (Savaki et al., 1984). Dopaminergic projection from the ventral tegmental area to the NAc is thought to be almost exclusively unilateral (Nauta et al., 1978), although recent studies revealed that some dopamine neurons project contralateral to their origin and showed cross-hemispheric synchronicity in dopamine signaling (Steinberg et al., 2014; Fox et al., 2016). Unilateral manipulations (lesioning, stimulation or pharmacological administration) of one nigrostriatal system were reported to affect gene expression, dopamine synthesis and turnover, and dopamine D1:D2 receptor interaction in contralateral structures (Leviel et al., 1979; Chéramy et al., 1983; Schwarting et al., 1996; Roedter et al., 2001; Lieu et al., 2012; Yano et al., 2006; Hyde et al., 1994). Bilateral functional compensations were also observed by cerebral blood flow-related tissue radioactivity after unilateral nigrostriatal damage (Yang et al., 2007). In addition, interhemispheric functional relationships of cortical neurons were reported using optogenetics and voltage-sensitive dye (Lim et al., 2012). fMRI studies after unilateral optogenetic stimulation of striatal neurons also showed bilateral effects (Lee et al., 2016). In line with these reports, our results indicate that unilateral increase in D1-SPN activity in the DS evokes a bilateral increase in neuronal activity in the prefrontal, somatosensory and motor cortices. These effects support a functional and compensatory interdependence between right and left DS-controlled networks.

A significant fALFF increase was observed in only a small area in the DS although the fALFF increased widely in the cortex. The small size of the area in which fALFF was increased in the DS is possibly related to several factors. First, it could be linked to inter-individual differences in the region infected by the Gq-DREADD-expressing AAV, as shown in Fig. 1E. The activation area detected by averaging fALFF data from all the animals corresponds to the area of overlap of Gq-DREADD expression in these mice, which appeared restricted (see Fig. 1E). Another factor could be related to the fact that the infected D1-SPNs are GABAergic inhibitory neurons, while the pyramidal neurons in the cortex are excitatory. It is likely that activation of GABAergic SPNs will tend to inhibit uninfected neighboring neurons, reducing the size of the activation area in the DS. In contrast, stimulation of excitatory neurons in the cortex could be expected to lead to an extension of the activation area.

Our study combining fMRI and electrophysiological measurements provides insights into the bases of the observed changes. In task-based fMRI following whisker stimulation, Mishra et al. showed negative correlation between BOLD signal change and neuronal activity in the striatum during spike-wave discharges in a rat model of epilepsy (Mishra et al., 2011). However, in the present study, the gamma BLP significantly increased in the regions in which fALFF also increased. This indicates that the observed increases of fALFF were likely caused by neural activity changes. Our results also showed that FC was not significantly altered by CLZ or CNO treatments. It should be noted that in a previous study no alteration of FC was observed during neuronal activation in the ventral tegmental area or NAc using DREADDs (Roelofs et al., 2017), similar to our results. Interestingly, zero-lag correlation (i.e., resting state FC) of BOLD fluctuation would be independent of the amplitude of infraslow-range activity (as evaluated via fALFF). The lack of effect on FC indicates that there is no significant change in phase between the signals in the various anatomically separated regions. Therefore, the current study highlights the importance to investigate different dimensions of resting state functioning and to confirm alterations in neuronal activity using other techniques including electrophysiology.

4.3. fALFF and BLP alteration

fALFF, which measures the relative contribution of low frequency band (0.01–0.1 Hz) to the whole frequency range of the fluctuation of rsfMRI signals, was shown to reflect spontaneous neural activity in the brain at basal state (Zou et al., 2008). In the present study, we used electrophysiology to identify the alterations of neuronal activity power in regions in which fALFF was changed following the Gq-DREADD-induced neuronal excitation. We confirmed that the total LFP was increased in left DS (Gq-DREADD-expressing area) after CLZ injection. Furthermore, the gamma bands in the left DS and in both left and right motor cortices were significantly increased following CLZ injection. Since previous rodent and primate studies showed that the gamma band power is associated with BOLD signals (Logothetis et al., 2001; Kayser et al., 2004; Niessing et al., 2005; Nir et al., 2007) and neuronal spiking activity (Buzsaki et al., 2012), increased fALFF in these areas suggested actual increases in

neuronal activity. In addition to the gamma band, we observed an increase in delta band power in the ipsilateral DS, but not in the motor cortex. Glutamate levels were reported to be related to the gamma band (Lally et al., 2014), while the effects of dopaminergic and cholinergic neuron stimulation have been observed on low frequency fluctuation of LFP (Neske, 2016). The delta power of LFP in the ipsilateral DS was reduced by dopamine disruption at resting state (Zhang et al., 2018). Although the mechanism of delta band power increase in the ipsilateral DS is not clear, dopaminergic or cholinergic neuron activation indirectly resulting from that of D1-SPNs may contribute to this effect. In addition, isoflurane was shown to be a selective enhancer of intrasynaptic $GABA_A$ receptor-mediated currents in rat hippocampus (Garcia et al., 2010). Since our Gq-DREADD stimulation targeted GABAergic SPNs in the DS, it is possible that the delta band power increase in DS reflected the interaction between the effects of SPN activation and isoflurane. In total, our results indicate that increased fALFF in the DS and motor cortex are derived from an actual increase of neuronal activity.

4.4. Limitations

The present study has several potential limitations. A first limitation could be linked to receptor desensitization with repeated DREADD activation that is one of the general concerns for chemogenetic technologies (Roth, 2016). In the current study, DREADDs were activated twice by CLZ or CNO in each animal to perform the behavior test before fMRI or LFP recordings. Receptor desensitization may influence results, such as the timing of CLZ effects determined from initial behavioral studies that may not be consistent for the latter fMRI and LFP recordings. However, we visually confirmed the existence of a rotation bias induced by CLZ just before anesthesia for fMRI. A second limitation is related to possible off-target effects of CLZ. CLZ has affinities for several endogenous receptors including serotonin, dopamine, α-adrenergic, muscarinic, and histamine receptors (Selent et al., 2008; Bonaventura et al., 2019). Furthermore, CLZ is reported to cause complex effects on ERK activation, mostly inhibition within the first few hours, probably by interacting with these various receptors (Pozzi et al., 2003; Pereira et al., 2012). Although we used a low dose of CLZ (0.1 mg/kg, i.p.) as recommended in a recent report (Gomez et al., 2017), CLZ at low doses (0.05–0.1 mg/kg, i.p.) is reported to affect some behavioral conditioning (Ilg et al., 2018). However, in our experiments, we did not observe any significant DREADD-independent effect of CLZ on pERK staining or behavioral responses (rotation bias and locomotion). In addition, we did not detect any significant CLZ effects on fMRI in several control mouse groups that did not express Gq-DREADD. These experiments establish that CLZ, at least at the low dose used in our experiments, is compatible with fMRI studies without confounding DREADD-independent effects. A third limitation is the possible effect of anesthesia with isoflurane on fMRI results. Isoflurane dose-dependently suppresses neuronal activity as well as neurovascular coupling, but it was demonstrated that 1.0% isoflurane, the maximum dose that we used in the present study, did not fully suppress neuronal activity in resting state or task-based neuronal activation (Tsurugizawa et al., 2016, 2019; Bukhari et al., 2017). Additionally, 1.0% isoflurane is useable to observe subcortical functional connectivity in mice (Zerbi et al., 2019) although it reduces the subcortical functional connectivity (Buckhari et al., 2017; Paasonen et al., 2018). In the present study, mice were anesthetized 25 min after saline or CLZ injection for fMRI to avoid the suppression of neuronal activity by long-lasting anesthesia. However, the limited total duration of anesthesia prevented us from studying fALFF changes as compared to baseline in each group. The mixture of medetomidine and isoflurane is generally considered as a better anesthesia protocol than isoflurane alone for rsfMRI (Grandjean et al., 2014; Paasonen et al., 2018). However, medetomidine anesthesia poses technical problems that are difficult to overcome. Particularly it is not suitable for checking the effects of DREADD stimulation on behavior before scanning because it takes 30–45 min for the induction of anesthesia. Chronic recording of neuronal activity and rsfMRI in freely moving awake animals could overcome the problem of anesthesia in future studies. Another limitation could be that our fALFF data were acquired using a brain segmentation approach because our fMRI resolution was too low to observe fALFF at sub nucleus-level (Supplementary Fig. 5A). To improve contrast and resolution, higher magnetic fields and higher quality coils (for example, cryoprobe) are required. This is the topic of our future work.

4.5. Perspectives and conclusions

Alterations in D1-SPNs are suspected to play a key role in the onset of PD symptoms (Mallet, 2006; Bergman, 1990). Optogenetic and chemogenetic manipulations of these neurons reinforce or alleviate PD symptoms in animal models (Kravitz et al., 2010; Alcacer et al., 2017). Therefore, our study by examining the effects of chemogenetic D1-SPN stimulation on whole brain activity is a first step towards a better understanding of their role in PD *in vivo* and their possible investigation in patients with non-invasive methods such as fMRI. Further studies using animal models of the disease are needed.

In conclusion, we successfully developed a chemo-fMRI system for the study of the DS network. We clarify how the type and dosage of pharmacological ligands for DREADD activation *in vivo* should be carefully chosen considering the possibility of DREADD-independent effects. We found bilateral effects with both fMRI and electrophysiological recordings following unilateral activation of DS direct pathway neurons. This approach should facilitate the comprehensive understanding of the whole brain network adaptation following selective alteration of specific neuron populations within the striatum. It will also contribute to the interpretation of cell type-specific activity changes on MRI images, helping to evaluate the progression of neurological diseases and to unravel the effect of pharmacological agents upon acute and chronic treatments.

CRediT authorship contribution statement

Yuki Nakamura: Conceptualization, Methodology, Investigation, Visualization, Writing - original draft. **Yukari Nakamura:** Investigation, Visualization. **Assunta Pelosi:** Investigation, Visualization. **Boucif Djemai:** Investigation. **Clément Debacker:** Investigation. **Denis Hervé:** Conceptualization, Supervision, Writing - review & editing. **Jean-Antoine Girault:** Conceptualization, Supervision, Writing - review & editing. **Tomokazu Tsurugizawa:** Conceptualization, Methodology, Investigation, Visualization, Supervision, Writing - review & editing.

Acknowledgments

Research in the laboratory of JAG was supported by Inserm and Sorbonne University and by grants from *Fondation pour la Recherche Médicale* (FRM, DPA20140629798) and ANR (Epitraces, ANR-16-CE16-0018). The project is also supported by the Fondation de France (grant number: 00086313, to DH). Equipment at the IFM was funded in part by *Fédération pour la recherche sur le cerveau* (FRC) and Rotary *Espoir en Tête*, and by DIM *Cerveau et Pensée Région Ile-de-France*. YN was recipient of a Uehara Memorial Foundation fellowship (201430033) and a Fyssen Foundation fellowship. Equipment for the electrophysiology studies was funded by the Idex Paris-Saclay. The authors thank Dr. Fiona Francis for kindly reading and correcting the manuscript.

Appendix A. Supplementary data

Supplementary data to this article can be found online at https://doi.org/10.1016/j.neuroimage.2020.117079.

References

Albin, R.L., Anne, B., Young, Penney, J.B., 1989. The functional anatomy of basal ganglia disorders. Trends Neurosci. 12, 366–375. https://doi.org/10.1016/0166-2236(89)90074-X.

Alcacer, C., et al., 2017. Chemogenetic stimulation of striatal projection neurons modulates responses to Parkinson's disease therapy. J. Clin. Invest. 127, 720–734. https://doi.org/10.1172/JCI90132.
Alexander, G.M., et al., 2009. Remote control of neuronal activity in transgenic mice expressing evolved G protein-coupled receptors. Neuron 63, 27–39. https://doi.org/10.1016/j.neuron.2009.06.014.
Armbruster, B.N., Li, X., Pausch, M.H., Herlitze, S., Roth, B.L., 2007. Evolving the lock to fit the key to create a family of G protein-coupled receptors potently activated by an inert ligand. Proc. Natl. Acad. Sci. U. S. A. 104, 5163–5168. https://doi.org/10.1073/pnas.0700293104.
Belin, D., Jonkman, S., Dickinson, A., Robbins, T.W., Everitt, B.J., 2009. Parallel and interactive learning processes within the basal ganglia: relevance for the understanding of addiction. Behav. Brain Res. 199, 89–102. https://doi.org/10.1016/j.bbr.2008.09.027.
Bergman, H., Wichmann, T., DeLong, M.R., 1990. Reversal of experimental parkinsonism by lesions of the subthalamic nucleus. Science 249, 1436–1438. https://doi.org/10.1126/science.2402638.
Bernal-Casas, D., Lee, H.J., Weitz, A.J., Lee, J.H., 2017. Studying brain circuit function with dynamic causal modeling for optogenetic fMRI. Neuron 93, 522–532. https://doi.org/10.1016/j.neuron.2016.12.035 e525.
Bonaventura, J., et al., 2019. High-potency ligands for DREADD imaging and activation in rodents and monkeys. Nat. Commun. 10, 4627. https://doi.org/10.1038/s41467-019-12236-z.
Boyden, E.S., Zhang, F., Bamberg, E., Nagel, G., Deisseroth, K., 2005. Millisecond-timescale, genetically targeted optical control of neural activity. Nat. Neurosci. 8, 1263–1268. https://doi.org/10.1038/nn1525.
Bukhari, Q., Schroeter, A., Cole, D.M., Rudin, M., 2017. Resting state fMRI in mice reveals anesthesia specific signatures of brain functional networks and their interactions. Front. Neural Circ. 11, 5. https://doi.org/10.3389/fncir.2017.00005.
Buzsáki, G., Anastassiou, C.A., Koch, C., 2012. The origin of extracellular fields and currents–EEG, ECoG, LFP and spikes. Nat. Rev. Neurosci. 13, 407–420. https://doi.org/10.1038/nrn3241.
Cenci, M.A., 2007. Dopamine dysregulation of movement control in L-DOPA-induced dyskinesia. Trends Neurosci. 30, 236–243. https://doi.org/10.1016/j.tins.2007.03.005.
Chéramy, A., Chesselet, M.F., Romo, R., Leviel, V., Glowinski, J., 1983. Effects of unilateral electrical stimulation of various thalamic nuclei on the release of dopamine from dendrites and nerve terminals of neurons of the two nigrostriatal dopaminergic pathways. Neuroscience 8, 767–780.
Chevalier, G., Deniau, J.M., 1990. Disinhibition as a basic process in the expression of striatal functions. Trends Neurosci. 13, 277–280. https://doi.org/10.1016/0166-2236(90)90109-n.
Christie, I.N., et al., 2013. fMRI response to blue light delivery in the naive brain: implications for combined optogenetic fMRI studies. Neuroimage 66, 634–641. https://doi.org/10.1016/j.neuroimage.2012.10.074.
DiFrancesco, M.W., et al., 2008. Comparison of SNR and CNR for in vivo mouse brain imaging at 3 and 7 T using well matched scanner configurations. Med. Phys. 35, 3972–3978. https://doi.org/10.1118/1.2968092.
Fox, M.E., et al., 2016. Cross-hemispheric dopamine projections have functional significance. Proc. Natl. Acad. Sci. U. S. A. 113, 6985–6990. https://doi.org/10.1073/pnas.1603629113.
Garcia, P.S., Kolesky, S.E., Jenkins, A., 2010. General anesthetic actions on GABA(A) receptors. Curr. Neuropharmacol. 8, 2–9. https://doi.org/10.2174/157015910790909502.
Gerfen, C.R., Surmeier, D.J., 2011. Modulation of striatal projection systems by dopamine. Annu. Rev. Neurosci. 34, 441–466. https://doi.org/10.1146/annurev-neuro-061010-113641.
Giorgi, A., et al., 2017. Brain-wide mapping of endogenous serotonergic transmission via chemogenetic fMRI. Cell Rep. 21, 910–918. https://doi.org/10.1016/j.celrep.2017.09.087.
Girault, J.A., Savaki, H.E., Desban, M., Glowinski, J., Besson, M.J., 1985. Bilateral cerebral metabolic alterations following lesion of the ventromedial thalamic nucleus: mapping by the 14C-deoxyglucosemethod in conscious Rats. J. Comp. Neurol. 231, 137–149. https://doi.org/10.1002/cne.902310202.
Gomez, J.L., et al., 2017. Chemogenetics revealed: DREADD occupancy and activation via converted clozapine. Science 357, 503–507. https://doi.org/10.1126/science.aan2475.
Gottlich, M., et al., 2013. Altered resting state brain networks in Parkinson's disease. PloS One 8, e77336. https://doi.org/10.1371/journal.pone.0077336.
Grandjean, J., Schroeter, A., Batata, I., Rudin, M., 2014. Optimization of anesthesia protocol for resting-state fMRI in mice based on differential effects of anesthetics on functional connectivity patterns. Neuroimage 102, 838–847. https://doi.org/10.1016/j.neuroimage.2014.08.043.
Groenewegen, H.J., Berendse, H.W., 1994. The specificity of the 'nonspecific' midline and intralaminar thalamic nuclei. TINS (Trends Neurosci.) 17, 52–57.
Guettier, J.M., 2009. A chemical-genetic approach to study G protein regulation of ß cell function in vivo. Proc. Natl. Acad. Sci. U. S. A. 106, 19197–19202. https://doi.org/10.1073/pnas.0906593106.
Hacker, C.D., Snyder, A.Z., Pahwa, M., Corbetta, M., Leuthardt, E.C., 2017. Frequency-specific electrophysiologic correlates of resting state fMRI networks. Neuroimage 149, 446–457. https://doi.org/10.1016/j.neuroimage.2017.01.054.
Herkenham, M., 1979. The afferent and efferent connections of the ventromedial thalamic nucleus in the rat. J. Comp. Neurol. 183, 487–518.
Huang, M., et al., 2017. Altered fractional amplitude of low frequency fluctuation associated with cognitive dysfunction in first-episode drug-naïve major depressive disorder patients. BMC Psychiatr. 17, 11. https://doi.org/10.1186/s12888-016-1190-1.
Hyde, J.F., VanderWende, C., Wood, P.L., Kim, H.F., Jerussi, T.P., 1994. Bilateral changes in striatal dopamine metabolism after unilateral intracarotid and intrastriatal administration of apomorphine. Brain Res. 655, 83–90.
Ilg, A.K., Enkel, T., Bartsch, D., Bahner, F., 2018. Behavioral effects of acute systemic low-dose clozapine in wild-type rats: implications for the Use of DREADDs in Behavioral Neuroscience. Front. Behav. Neurosci. 12, 173. https://doi.org/10.3389/fnbeh.2018.00173.
Kravitz, A.V., et al., 2010. Regulation of parkinsonian motor behaviours by optogenetic control of basal ganglia circuitry. Nature 466, 622–626. https://doi.org/10.1038/nature09159.
Kayser, C., Kim, M., Ugurbil, K., Kim, D.S., Konig, P., 2004. A comparison of hemodynamic and neural responses in cat visual cortex using complex stimuli. Cerebr. Cortex 14, 881–891. https://doi.org/10.1093/cercor/bhh047.
Kuramoto, E., et al., 2011. Complementary distribution of glutamatergic cerebellar and GABAergic basal ganglia afferents to the rat motor thalamic nuclei. Eur. J. Neurosci. 33, 95–109. https://doi.org/10.1111/j.1460-9568.2010.07481.x.
Kuramoto, E., et al., 2015. Ventral medial nucleus neurons send thalamocortical afferents more widely and more preferentially to layer 1 than neurons of the ventral anterior-ventral lateral nuclear complex in the rat. Cerebr. Cortex 25, 221–235. https://doi.org/10.1093/cercor/bht216.
Lally, N., et al., 2014. Glutamatergic correlates of gamma-band oscillatory activity during cognition: a concurrent ER-MRS and EEG study. Neuroimage 85 (Pt 2), 823–833. https://doi.org/10.1016/j.neuroimage.2013.07.049.
Lee, H.J., et al., 2016. Activation of direct and indirect pathway medium spiny neurons drives distinct brain-wide responses. Neuron 91, 412–424. https://doi.org/10.1016/j.neuron.2016.06.010.
Leviel, V., Chéramy, A., Nieoullon, A., Glowinski, J., 1979. Symmetric bilateral changes in dopamine release from the caudate nuclei of the cat induced by unilateral nigral application of glycine and gaba-related compounds. Brain Res. 175, 259–270.
Lieu, C.A., Subramanian, T., 2012. The interhemispheric connections of the striatum: implications for Parkinson's disease and drug-induced dyskinesias. Brain Res. Bull. 87, 1–9. https://doi.org/10.1016/j.brainresbull.2011.09.013.
Lim, D.H., et al., 2012. In vivo large-scale cortical mapping using channelrhodopsin-2 stimulation in transgenic mice reveals asymmetric and reciprocal relationships between cortical areas. Front. Neural Circ. 6, 11. https://doi.org/10.3389/fncir.2012.00011.
Logothetis, N.K., Pauls, J., Augath, M., Trinath, T., Oeltermann, A., 2001. Neurophysiological investigation of the basis of the fMRI signal. Nature 412, 150–157.
Luo, C.Y., et al., 2015. Functional connectome assessed using graph theory in drug-naive Parkinson's disease. J. Neurol. 262, 1557–1567. https://doi.org/10.1007/s00415-015-7750-3.
Ma, Y., et al., 2016. Resting-state hemodynamics are spatiotemporally coupled to synchronized and symmetric neural activity in excitatory neurons. Proc. Natl. Acad. Sci. U. S. A. 113, E8463–E8471. https://doi.org/10.1073/pnas.1525369113.
MacLaren, D.A., et al., 2016. Clozapine N-oxide administration produces behavioral effects in long-evans rats: implications for designing DREADD experiments. eNeuro 3. https://doi.org/10.1523/ENEURO.0219-16.2016.
Mallet, N., Ballion, B., Le Moine, C., Gonon, F., 2006. Cortical inputs and GABA interneurons imbalance projection neurons in the striatum of parkinsonian rats. J. Neurosci. 26, 3875–3884. https://doi.org/10.1523/JNEUROSCI.4439-05.2006.
Mishra, A.M., et al., 2011. Where fMRI and electrophysiology agree to disagree: corticothalamic and striatal activity patterns in the WAG/Rij rat. J. Neurosci. 31, 15053–15064. https://doi.org/10.1523/JNEUROSCI.0101-11.2011.
Mitchell, A.S., Chakraborty, S., 2013. What does the mediodorsal thalamus do? Front. Syst. Neurosci. 7, 37. https://doi.org/10.3389/fnsys.2013.00037.
Murer, M.G., Moratalla, R., 2011. Striatal signaling in L-DOPA-induced dyskinesia: common mechanisms with drug abuse and long term memory involving D1 dopamine receptor stimulation. Front. Neuroanat. 5, 51. https://doi.org/10.3389/fnana.2011.00051.
Nagano-Saito, A., Martinu, K., Monchi, O., 2014. Function of basal ganglia in bridging cognitive and motor modules to perform an action. Front. Neurosci. 8, 187. https://doi.org/10.3389/fnins.2014.00187.
Nauta, W.J.H., Smith, G.P., Faull, R.L.M., Domesick, V.B., 1978. Efferent connections and nigral afferents of the nucleus accumbens septi in the rat. Neuroscience 3, 385–401.
Nelson, A.B., Kreitzer, A.C., 2014. Reassessing models of basal ganglia function and dysfunction. Annu. Rev. Neurosci. 37, 117–135. https://doi.org/10.1146/annurev-neuro-071013-013916.
Neske, G.T., 2016. The slow oscillation in cortical and thalamic networks: mechanisms and functions. Front Neural Circuits. 9, 88. https://doi.org/10.3389/fncir.2015.00088.
Niessing, J., et al., 2005. Hemodynamic signals correlate tightly with synchronized gamma oscillations. Science 309, 948–951. https://doi.org/10.1126/science.1110948.
Nir, Y., et al., 2007. Coupling between neuronal firing rate, gamma LFP, and BOLD fMRI is related to interneuronal correlations. Curr. Biol. 17, 1275–1285. https://doi.org/10.1016/j.cub.2007.06.066.
Owen, S.F., Liu, M.H., Kreitzer, A.C., 2019. Thermal constraints on in vivo optogenetic manipulations. Nat. Neurosci. 22, 1061–1065. https://doi.org/10.1038/s41593-019-0422-3.
Paasonen, J., Stenroos, P., Salo, R.A., Kiviniemi, V., Grohn, O., 2018. Functional connectivity under six anesthesia protocols and the awake condition in rat brain. Neuroimage 172, 9–20. https://doi.org/10.1016/j.neuroimage.2018.01.014.

Pereira, A., et al., 2012. Clozapine induction of ERK1/2 cell signalling via the EGF receptor in mouse prefrontal cortex and striatum is distinct from other antipsychotic drugs. Int. J. Neuropsychopharmacol. 15, 1149–1160. https://doi.org/10.1017/S1461145711001404.

Pozzi, L., et al., 2003. Opposite regulation by typical and atypical anti-psychotics of ERK1/2, CREB and Elk-1 phosphorylation in mouse dorsal striatum. J. Neurochem. 86, 451–459. https://doi.org/10.1046/j.1471-4159.2003.01851.x.

Power, J.D., Barnes, K.A., Snyder, A.Z., Schlaggar, B.L., Petersen, S.E., 2013. Steps toward optimizing motion artifact removal in functional connectivity MRI; a reply to Carp. Neuroimage 76, 439–441. https://doi.org/10.1016/j.neuroimage.2012.03.017.

Roedter, A., et al., 2001. Comparison of unilateral and bilateral intrastriatal 6-Hydroxydopamine-induced axon terminal lesions: evidence for interhemispheric functional coupling of the two nigrostriatal pathways. J. Comp. Neurol. 432, 217–229.

Roelofs, T.J.M., et al., 2017. A novel approach to map induced activation of neuronal networks using chemogenetics and functional neuroimaging in rats: a proof-of-concept study on the mesocorticolimbic system. Neuroimage 156, 109–118. https://doi.org/10.1016/j.neuroimage.2017.05.021.

Rolinski, M., et al., 2015. Aberrant functional connectivity within the basal ganglia of patients with Parkinson's disease. Neuroimage Clin. 8, 126–132. https://doi.org/10.1016/j.nicl.2015.04.003.

Roth, B.L., 2016. DREADDs for neuroscientists. Neuron 89, 683–694. https://doi.org/10.1016/j.neuron.2016.01.040.

Rungta, R.L., Osmanski, B.F., Boido, D., Tanter, M., Charpak, S., 2017. Light controls cerebral blood flow in naive animals. Nat. Commun. 8, 14191. https://doi.org/10.1038/ncomms14191.

Savaki, H.E., Girault, J.-A., Desban, M., Glowlnski, J., Besson, M.-J., 1984. Basal ganglia and related motor structures. Brain Res. Bull. 12, 609–616.

Schaber, G., Stevens, I., Gaertner, H.J., Dietz, K., Breyer-Pfaff, U., 1998. Pharmacokinetics of clozapine and its metabolites in psychiatric patients: plasma protein binding and renal clearance. Br. J. Clin. Pharmacol. 46, 453–459. https://doi.org/10.1046/j.1365-2125.1998.00822.x.

Schmid, F., et al., 2017. True and apparent optogenetic BOLD fMRI signals. Magn. Reson. Med. 77, 126–136. https://doi.org/10.1002/mrm.26095.

Schwarting, R.K.W., Huston, J.P., 1996. Unilateral 6-hydroxydopamine lesions of mesostriatal dopamine neurons and their physiological sequelae. Prog. Neurobiol. 49, 215–266.

Seehafer, J.U., et al., 2010. No increase of the blood oxygenation level-dependent functional magnetic resonance imaging signal with higher field strength: implications for brain activation studies. J. Neurosci. 30, 5234–5241. https://doi.org/10.1523/JNEUROSCI.0844-10.2010.

Selent, J., Lopez, L., Sanz, F., Pastor, M., 2008. Multi-receptor binding profile of clozapine and olanzapine: a structural study based on the new beta2 adrenergic receptor template. ChemMedChem 3, 1194–1198. https://doi.org/10.1002/cmdc.200800074.

Sierakowiak, A., Monnot, C., Aski, S.N., Uppman, M., Li, T.Q., Damberg, P., Brené, S., 2015. Default mode network, motor network, dorsal and ventral basal ganglia networks in the rat brain: comparison to human networks using resting state-fMRI. PloS One, e0120345. https://doi.org/10.1371/journal.pone.0120345.

Smith, Y., et al., 2014. The thalamostriatal system in normal and diseased states. Front. Syst. Neurosci. 8, 5. https://doi.org/10.3389/fnsys.2014.00005.

Song, X.W., et al., 2011. REST: a toolkit for resting-state functional magnetic resonance imaging data processing. PloS One 6, e25031. https://doi.org/10.1371/journal.pone.0025031.

Steinberg, E.E., et al., 2014. Positive reinforcement mediated by midbrain dopamine neurons requires D1 and D2 receptor activation in the nucleus accumbens. PloS One 9, e94771. https://doi.org/10.1371/journal.pone.0094771.

Tepper, J.M., Abercrombie, E.D., Bolam, J.P., 2007. Basal ganglia macrocircuits. Prog. Brain Res. 160, 3–7. https://doi.org/10.1016/S0079-6123(06)60001-0.

Thompson, G.J., et al., 2013. Neural correlates of time-varying functional connectivity in the rat. Neuroimage 83, 826–836. https://doi.org/10.1016/j.neuroimage.2013.07.036.

Tsurugizawa, T., Takahashi, Y., Kato, F., 2016. Distinct effects of isoflurane on basal BOLD signals in tissue/vascular microstructures in rats. Sci. Rep. 6, 38977. https://doi.org/10.1038/srep38977.

Tsurugizawa, T., Djemai, B., Zalesky, A., 2019. The impact of fasting on resting state brain networks in mice. Sci. Rep. 9, 2976. https://doi.org/10.1038/s41598-019-39851-6.

Turner, J.A., et al., 2013. A multi-site resting state fMRI study on the amplitude of low frequency fluctuations in schizophrenia, 2013 schizophrenia. Front. Neurosci. 7, 137. https://doi.org/10.3389/fnins.2013.00137.

Valjent, E., Corvol, J.C., Pagés, C., Besson, M.J., Maldonado, R., Caboche, J., 2000. Involvement of the extracellular signal-regulated kinase cascade for cocaine-rewarding properties. J. Neurosci. 20, 8701–8709. https://doi.org/10.1523/JNEUROSCI.20-23-08701.2000.

Valjent, E., Bertran-Gonzalez, J., Herve, D., Fisone, G., Girault, J.A., 2009. Looking BAC at striatal signaling: cell-specific analysis in new transgenic mice. Trends Neurosci. 32, 538–547. https://doi.org/10.1016/j.tins.2009.06.005.

Wei, L., et al., 2014. Reduced topological efficiency in cortical-basal Ganglia motor network of Parkinson's disease: a resting state fMRI study. PloS One 9, e108124. https://doi.org/10.1371/journal.pone.0108124.

Wu, T., et al., 2015. Parkinson's disease—related spatial covariance pattern identified with resting-state functional MRI. J. Cerebr. Blood Flow Metabol. 35, 1764–1770. https://doi.org/10.1038/jcbfm.2015.118.

Xue, J., et al., 2017. Age of acquisition effects on word processing for Chinese native learners' English: ERP evidence for the Arbitrary Mapping Hypothesis. Front. Psychol. 8, 818. https://doi.org/10.3389/fpsyg.2017.00818.

Yang, J., Sadler, T.R., Givrad, T.K., Maarek, J.-M.I., Holschneider, D.P., 2007. Changes in brain functional activation during resting and locomotor states after unilateral nigrostriatal damage in rats. Neuroimage 36, 755–773. https://doi.org/10.1016/j.neuroimage.2007.03.010.

Yano, M., Beverley, J.A., Steiner, H., 2006. Inhibition of methylphenidate-induced gene expression in the striatum by local blockade of D1 dopamine receptors: interhemispheric effects. Neuroscience 140, 699–709. https://doi.org/10.1016/j.neuroscience.2006.02.017.

Zerbi, V., et al., 2019. Rapid reconfiguration of the functional connectome after chemogenetic locus coeruleus activation. Neuron 103, 702–718. https://doi.org/10.1016/j.neuron.2019.05.034 e705.

Zhang, H., et al., 2018. Altered local field potential relationship between the parafascicular thalamic nucleus and dorsal striatum in hemiparkinsonian rats. Neurosci. Bull. https://doi.org/10.1007/s12264-018-0312-9.

Zou, Q.H., et al., 2008. An improved approach to detection of amplitude of low-frequency fluctuation (ALFF) for resting-state fMRI: fractional ALFF. J. Neurosci. Methods 172, 137–141. https://doi.org/10.1016/j.jneumeth.2008.04.012.